From torsional spectra to Hamiltonians and dynamics: effects of coupled bright and dark states of 9-(N-carbazolyl)-anthracene

J. Manz, B. Proppe, B. Schmidt

Institut für Physikalische und Theoretische Chemie, Freie Universität Berlin, Takustrasse 3, D-14195 Berlin, Germany

Abstract. The torsional dynamics of the 9-(N-carbazolyl)-anthracene (C9A) molecule is investigated by means of time-independent (1) and time-dependent (2) quantum-mechanical simulations in a diabatic representation. The study includes effects of surface crossing of the bright S_1 state with a dark state. (1) The intensity pattern of the $S_0 \to S_1$ fluorescence excitation spectrum is used to fit an effective one-dimensional Hamiltonian with a single-minimum potential for the dark state together with diabatic couplings to the double well potential of the bright state. (2) Based on this Hamiltonian, first predictions for a pump-probe scheme are made. In the pump process the molecules are excited to the S_1 state followed by competing torsions in the bright state and diabatic curve crossings to the dark state, depending on the pump frequency. Assuming the probe process to be an ionization from the bright state, the interfering effects of the dark state on the dynamics in the bright state can be monitored in a directly time-dependent way on a fs-ps time scale.

PACS: 33.10.-n; 33.50.Hv; 33.80.Be

1 Introduction

The process of photoinduced twisting of molecular bonds is of fundamental importance in organic photochemistry [1]. An interesting class of phenomena arises where the torsion of a single or double bond couples different electronic states which can lead to intersections (photochemical funnels) of potential surfaces. Torsional photoisomerizations involving excited states with charge separation are of particular relevance. Since the early days of its foundation [2, 3], the "Twisted Intramolecular Charge Transfer" (TICT) model has been subject of numerous publications (see, e.g. [4, 5] and references therein).

A class of molecules which has been investigated in great detail are aromatic double molecules like bianthryl [6]. For this symmetric molecule, the charge-separated

nature of the excited state has already been verified for solvent-solute clusters [7, 8]. TICT formation is more likely for an asymmetric donor-acceptor compound. This asymmetry can be introduced by replacing one of the anthryl moieties by a strong donor like a carbazolyl group (see Fig. 1). In a recent study, Monte et al. investigated the torsional structure of 9-(N-carbazolyl)-anthracene (C9A) in a supersonic nozzle beam [9]. The main focus of their investigation is on high-resolution fluorescence spectroscopy of a transition between the electronic ground state (S_0) and the first excited state (S_1) which corresponds essentially to a local excitation of the anthryl part of C9A. In this spectral region the fluorescence excitation spectrum shows a long torsional progression extending over $1000 \, cm^{-1}$ from the 0–0 transition at $25893.3 \, cm^{-1}$ (see Fig. 2). However, the intensity profile exhibits a remarkable minimum in the center of the progression which could not be accounted for by the S_0 and S_1 potentials fitted to the dispersed fluorescence spectra. This peculiarity was attributed to the effect of a resonant nonradiative coupling to a "dark" state. This conjecture is further confirmed by fluorescence lifetime measurements. The quantum-chemical nature of this "S_x" state is still unknown but is likely to be a TICT state [9].

In the present paper we investigate the effects of coupling of bright (S_1) and dark states (S_x) further using an effective one-dimensional model Hamiltonian based on a diabatic representation of the electronic states and couplings
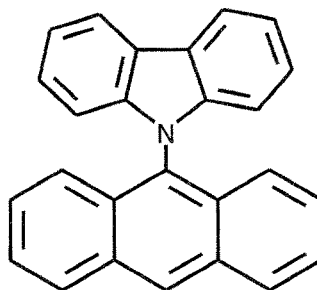

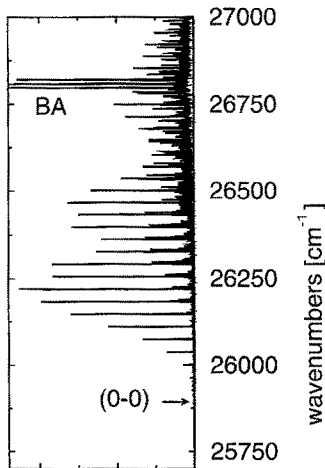Fig. 1. Structure of the 9-(N-carbazolyl)-anthracene (C9A) molecule

Fig. 2. Experimental fluorescence excitation spectrum of C9A in the region of the $S_0 \rightarrow S_1$ excitation [9]. The *lines* denoted as BA are due to a bianthryl impurity of the substance. The *arrow* indicates the position of the 0–0 transition at 25893.3 cm^{-1}

(see Sect. 2). Computational details are explained in Sect. 3. The Hamiltonian is determined by approximate time-independent calculations of fluorescence excitation spectra (Sect. 4). Then this Hamiltonian is used for propagations of wave packets in order to simulate time-dependent spectra of a proposed pump-probe scheme as described in Sect. 5. Our overall strategy thus follows the general approach from time-independent spectra via effective Hamiltonians to time-dependent dynamics which was advocated by M. Quack [10, 11]. Section 5 summarizes our results and gives an outlook.

2 Model Hamiltonian

In the present study we describe the photochemical dynamics of the C9A molecule in the framework of an effective one-dimensional model Hamiltonian employing the torsional degree of freedom of twisting about the C–N axis, only. This simplification can be rationalized for two different reasons. First, because of the low frequency, torsional vibrations can be approximately separated from the other modes of vibration [9]. Second, the twisting of double molecules is known to be most effective in mediating degeneracies of electronic states like the S_1/S_x intersection to be investigated here [1]. This is due to the fact that torsional motion affects the interaction of the π-systems of the anthryl and carbazolyl parts most strongly. Similar effective low-dimensional Hamiltonians to model the torsional dynamics of large molecules can be found in the literature [12].

Neglecting the small dependence of the reduced moment of inertia I_{red} on the twisting angle ϕ (we adapt the constant value of $\hbar/(4\pi c I_{red}) = 0.035$ cm^{-1} as given in [9]), the diagonal elements of the molecular Hamiltonian for the torsional dynamics of the i-th electronic state can be written as [13]

$$H^{(i)}_{mol}(\phi) = -\frac{\hbar^2}{2I_{red}}\frac{\partial^2}{\partial\phi^2} + V^{(i)}(\phi) \tag{1}$$

where $V^{(i)}(\phi)$ denotes the effective torsional potential of the respective state. To incorporate electronic degrees of freedom into our model, we choose a diabatic representation of electronic states thus avoiding the effects of kinetic couplings. Similar approaches have been used in theoretical study of the twisting dynamics of small polyenes by Dormans et al. [14] and, more recently, by Seidner et al. in a multi-dimensional approach [15, 16]. In this picture, there are two different mechanisms of coupling between the various electronic states. First, as a consequence of the diabatic representation of the electronic states, there are off-diagonal elements $V^{(ij)}(\phi)$ in the potential matrix which couple the different states. Second, the electronic states may be coupled radiatively to each other. In semiclassical dipole approximation, the contribution of the light matter interaction to the Hamiltonian is described by

$$H^{(ij)}_{rad}(\phi, t) = -\varepsilon(t)\cdot\mu^{(ij)}(\phi) \tag{2}$$

where $\mu^{(ij)}(\phi)$ represents the transition dipole moment between state i and j, and $\varepsilon(t)$ gives the external electric field of radiation. In the following, we constrain ourselves to the three (diabatic) states S_0, S_1, and S_x for the electronic ground state, the first electronically excited (bright) state, and for the unknown "dark state", respectively. Thus, the total Hamiltonian for the torsional dynamics of a C9A molecule interacting with an external field can be written as

$$H_{tot}(\phi,t) = \begin{pmatrix} H^{(0)}_{mol}(\phi) & H^{(01)}_{rad}(\phi,t) & 0 \\ H^{(01)}_{rad}{}'(\phi,t) & H^{(1)}_{mol}(\phi) & V^{(1x)}(\phi) \\ 0 & V^{(1x)}(\phi) & H^{(x)}_{mol}(\phi) \end{pmatrix}. \tag{3}$$

In this approximation, diabatic couplings are taken into account only between the (intersecting) S_1 and S_x states neglecting all other potential couplings because of the large energy gaps between the ground state S_0 and each of the two excited states S_1 and S_x which are in the order of 26000 cm^{-1}. We also assume that radiative coupling occurs only between the S_0 and the bright S_1 state while the S_x state is assumed to be dark. This is plausible for charge transfer states which are known to carry no significant oscillator strength because there is no experimental observation of dual fluorescence for C9A. Furthermore, we assume that the electric field $\varepsilon(t)$ is polarized along the transition dipole moment $\mu^{(01)}(\phi)$.

3 Computational details

In the following we describe numerical methods used for the quantum-mechanical simulation of time-independent and time-dependent spectra. In either case we represent a wave function as a vector whose components are the values of the function on a discretized grid of equidistant points in coordinate space. Then the evaluation of a Hamiltonian like the one given in (1) acting on such a vector is particularly simple [17]. In this representation, the operator of the potential energy is local and the effect of the Laplacian in the kinetic energy operator can be calculated by forward and reverse Fourier transformation using efficient FFT-methods. A generalization of this method to wave functions on N coupled

electronic surfaces (cf. 3) is straightforward by assembling N state vectors to one vector which is N times longer and which represents the total wave function. In the present study we use a grid of 128 points ranging from 0.524 rad (30°) to 2.618 rad (150°) to discretize the torsional coordinate ϕ.

The computations can be made more efficient by explicitly taking into account the molecular symmetry. In the C_{2v} point group the torsional coordinate of the C9A molecule transforms like the irreducible representation a_2 and the torsional potentials and couplings are symmetric with respect to inversion at $\phi = \pi/2$. Hence, only symmetric (a_1) and antisymmetric (a_2) vibrational wave functions can be coupled to each other. Therefore, wave functions with even and odd quantum numbers can be treated independently.

For the calculation of absorption spectra (see Sect. 4) the time-independent Schrödinger equation is solved. We use the grid methods outlined above to obtain a matrix representation of the Hamiltonian. Diagonalization then yields the desired eigenvalues and eigenstates [18, 19]. The Hamiltonian is set up for two subspaces of the total space spanned by the wave functions in the three electronic states, (1) for the electronic ground state (S_0) alone and (2) for the coupled S_1 and S_x states. Diagonalization of the latter yields a manifold of excited state wave functions which can be interpreted as superpositions of vibrational wave functions in the S_1 state and in the S_x state. Then absorption spectra are calculated based on the Condon-approximation assuming a constant transition dipole moment $\mu^{(01)} = 1ea_0$. Relative spectral intensities are calculated as the squares of the Franck-Condon factors which are obtained as overlaps of the electronic ground state wave functions with the components of the excited states corresponding to vibrational wave functions in the bright S_1 state.

The simulation of pump-probe spectra in Sect. 5 requires the solution of the time-dependent Schrödinger equation. In the last years there has been intense work on the development of propagation algorithms based on grid representations [20, 21]. For the choice of the most efficient technique we have to consider two cases: For the C9A molecule interacting with a (pump) laser pulse we are dealing with a time-dependent Hamiltonian where the split-operator technique introduced by Feit et al. [22, 23] is found most appropriate. Note that for a problem with coupled potential surfaces such as in (3) we use a variant of this method developed by Alvarellos and Metiu [24]. For the numerical treatment of the laser pulses discussed in Sect. 5, this algorithm allows us to propagate with a time step of 0.05 fs. For the long time propagation in case of vanishing radiative coupling (delay time between pump and probe pulse) we use a method introduced by Tal-Ezer and Kosloff which is based on an expansion of the time evolution operator in a series of complex Chebychev polynomials [17, 25]. For a choice of the time step of 200 fs a total number of 170 polynomials has to be evaluated.

4 Potential functions and couplings

Our determination of the model Hamiltonian for C9A starts from the torsional band assignment of both fluorescence excitation and dispersed fluorescence spectra by Monte et al.
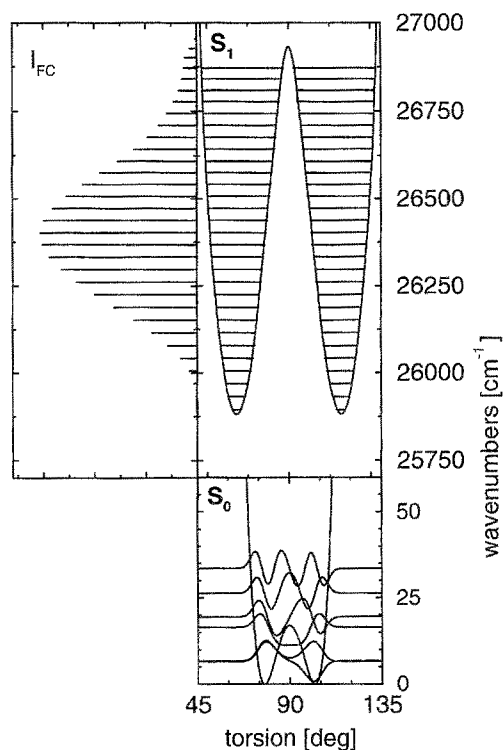

Fig. 3. The *right panel* shows the diabatic S_0 and the S_1 torsional potentials and vibrational energy levels of C9A (Note the different scales!). The *left part* of the figure shows the calculated Franck–Condon absorption spectrum for the $S_0 \to S_1$ transition (adapted from [9])

[9]. Analyzing the characteristic patterns of the Franck-Condon factors [6], effective potentials for the S_0 and S_1 states could be determined in a fitting procedure. Both potentials exhibit a double minimum structure along the torsional coordinate ϕ as can be seen in Fig. 3. With respect to a coplanar structure, the minimum energy geometries are twisted about the C–N axis by $\pi/2 \pm 0.218$ (77.5°, 102.5°) and $\pi/2 \pm 0.454$ (64°, 116°) for the S_0 and S_1 state, respectively. The potential barrier heights for perpendicularity ($\phi = \pi/2$) differ by almost two orders of magnitude. They are 17 cm^{-1} for the ground state (S_0) and 1050 cm^{-1} for the first excited state (S_1). Consequently, only the first pair of vibrational eigenstates which is well below the barrier of the S_0 potential is nearly degenerate. In the S_1 state, due to the much higher barrier, the first thirty levels are practically degenerate.

A Franck-Condon (absorption) spectrum for $S_0(v = 0)$ $\to S_1$ transitions based on these two potentials is also shown in Fig. 3. Due to the flatness of the S_0 potential there is a large Franck-Condon region resulting in a wide torsional progression up to an excess energy of ≈ 1000 cm^{-1} with line spacings of approximately 35 cm^{-1}. According to a reflection principle, the envelope of the intensities reflects the uninodal structure of the ground state wave function in each of the S_0 minima [6].

Although the line positions and the overall envelope of the torsional progression are in good agreement with the experimental spectrum of Fig. 2, there is a remarkable difference in the intensity profile. The experimental fluorescence excitation spectrum exhibits a pronounced minimum

around 26300 cm^{-1}. This discrepancy is used here to determine an effective potential for the "dark" S_x state. For this purpose, we approximate the fluorescence excitation spectrum by an absorption spectrum including the effect of diabatic coupling of the bright S_1 state to the dark S_x state as described in Sect. 2. We simulate "cold" spectra by assuming that only the doublet of the vibrational ground state is occupied and that the population of the symmetric (a_1) and antisymmetric (a_2) level is equal. Then the corresponding two absorption spectra are superimposed. In order to make them comparable to the experimental resolution, the spectra are broadened by folding the theoretical stick spectrum with a Gaussian of 3 cm^{-1} width (FWHM).

As proposed by Monte et al., the potential for the S_x state is assumed to have a single minimum at $\phi = \pi/2$. This is because the narrow region of the resonance can be explained best by a large difference of the slopes of the S_1 and S_x potentials at the intersection points [9]. For simplicity we choose a quartic potential with three fit parameters

$$V^{(x)}(\phi) = V_0 + \frac{1}{2}V_2\left(\phi - \frac{\pi}{2}\right)^2 + \frac{1}{24}V_4\left(\phi - \frac{\pi}{2}\right)^2 \qquad (4)$$

where V_0 stands for the vertical offset (with respect to the minimum of the S_0 potential) and V_2 and V_4 are the harmonic and quartic force constants, respectively. The diabatic potential coupling $V^{(1x)}(\phi)$ between the S_1 and S_x state is modelled here by two Gaussians centered at the crossing points of the two potential curves at $\pi/2 - \phi_0$ and $\pi/2 + \phi_0$

$$V^{(1x)}(\phi) = C\left\{\exp\left[-\frac{(\phi - \pi/2 + \phi_0)^2}{2a^2}\right]\right.$$
$$\left. + \exp\left[-\frac{(\phi - \pi/2 - \phi_0)^2}{2a^2}\right]\right\} \qquad (5)$$

where C and a determine the height and the width of these functions.

Our strategy to fit the parameters proceeds as follows. Based on a first reasonable guess of $V^{(x)}(\phi)$, the width and the height of the coupling of the two excited states S_1 and S_x are fit to reproduce the width and the depth of the minimum of the experimental intensity profile superimposed on the regular progression as shown in Fig. 2. In this way, the two parameters of $V^{(1x)}(\phi)$ given in (5) can be determined to be $C/(hc) = 22$ cm^{-1} for the coupling strength and $a = 0.056$ rad (3.2°) for the width of the Gaussian functions. These two values are kept constant throughout the fitting procedure of the S_x potential given in (4). Next the (inner) intersection points of the double minimum potential of the S_1 state and the parabola describing the S_x state are determined by fitting the position of the minimum of the experimental spectrum. This yields a value of $\phi_0 = 0.227$ rad (13°). Then the horizontal offset V_0 of the S_x parabola is fixed keeping the intersection points constant. First fits using a quadratic potential showed that this model did not offer enough flexibility to fit the details of the spectrum satisfactorily. This was improved by introducing the quartic term into (4). Thus, in the final procedure, we have a two-parametric fit for the three parameters V_0, V_2, and V_4 subject to one constraint.

Our results for the potentials and the corresponding Franck-Condon spectra are shown in Figs. 4 and 5, the
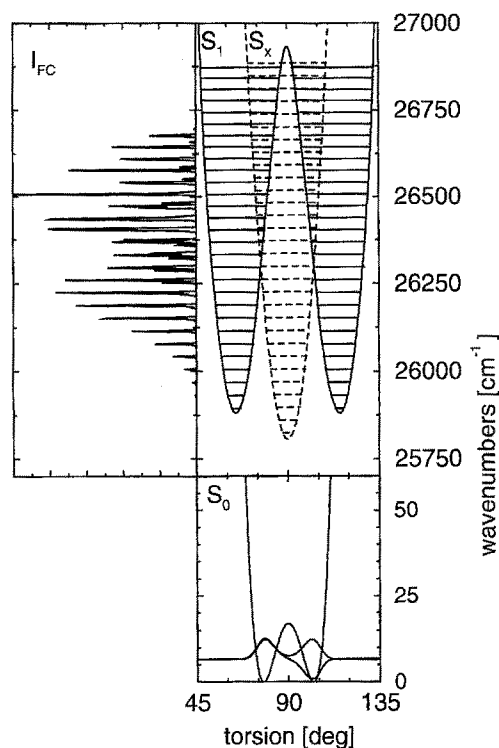

Fig. 4. Effect of the surface crossing. The *upper right part* shows the fit a) of the S_x potential together with the S_1 potential and the corresponding vibrational energy levels (see (4) and Table 1). The *left panel* shows the calculated Franck-Condon spectrum

values of the potential parameters are summarized in Table 1. While the parameters C and a as well as ϕ_0 can be fitted uniquely, there is some uncertainty in the choice of the remaining parameters. The two curves labelled as a) and b) represent lower and upper bounds with respect to the horizontal position of the vertex of the potential curve of the S_x state. Although the spectra can not be reproduced exactly it can be concluded that the overall agreement of experimental and theoretical intensity pattern is satisfactory, in particular for the levels in the lower energy range, $E \le 26300$ cm^{-1}. For higher energies the potential coupling becomes more important. In this region it is not possible to fit the experimental intensities with a similar precision using the simple models of (4) and (5). Furthermore, one expects more significant deviations between fluorescence excitation and absorption spectra due to more efficient energy redistribution in the time interval between the excitation and the fluorescence events which is beyond our simplified one-dimensional model. Moreover, there is some uncertainty in the experimental intensities over the complete spectral range.

Apart from modifying the intensity profile, there are two other marginal effects caused by the diabatic surface crossing. First, the degeneracy of symmetric (a_1) and antisymmetric (a_2) vibrational levels of the S_1 state is slightly lifted. However, these splittings of the doublets which reach a maximum of 3 cm^{-1} close to the intersection of the potential curves could not be detected in the experimental spectrum in Fig. 2. A second interesting feature of the non-radiative coupling is the effect of intensity borrowing. Reciprocal to the decrease of intensity for excitation to the S_1 levels there is
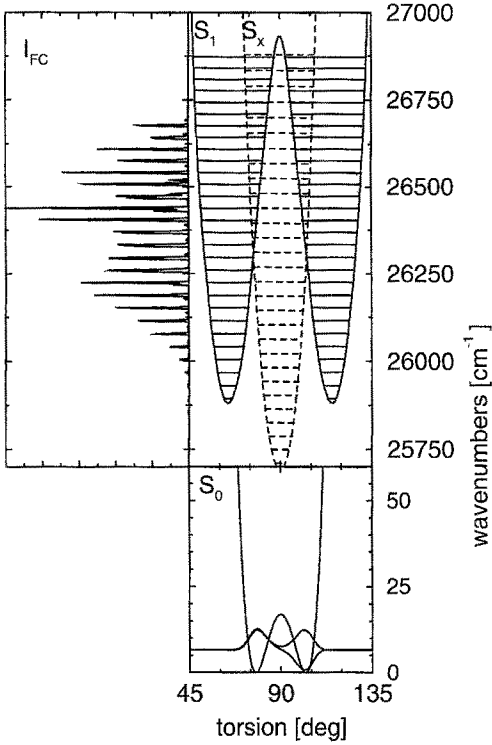
Fig. 5. Same as in Fig. 4 but for fit b) of the S_x potential (see (4) and Table 1)

Table 1. Fit parameters of the torsional potential $V^{(x)}$ of the dark S_x state and of the potential coupling $V^{(1x)}$ to the bright S_1 state as defined in (4) and (5), respectively. The columns a and b give two different fits for the potential parameters of the S_x potential (see Figs. 4 and 5)

	a	b
$V_0/(hc)$ [cm^{-1}]	25806	25691
$V_2/(hc)$ [cm^{-1}/rad^2]	19094	20192
$V_4/(hc)$ [cm^{-1}/rad^4]	0	797417
$C/(hc)$ [cm^{-1}]	22	22
a [rad]	0.056	0.056
ϕ_0 [rad]	0.227	0.227

an increase of intensity for excitations into levels associated with the S_x state. Due to the coupling to the S_1 state, this leads to additional lines in the calculated absorption spectra of Figs. 4 and 5 whose intensity reaches up to 20% of the strongest S_1 excitations. These lines are not present in the experimental fluorescence excitation spectrum (see our discussion in Sect. 6).

5 A pump-probe scheme

The effective torsional Hamiltonian which has been derived from the time-independent spectra in Sect. 4 can now be used to predict the time-dependent torsional dynamics of the C9A molecule. Specifically, we are interested in predicting some effects of the hypothetical dark S_x state on the dynamics in the S_1 state which should be observable in fs pump-probe

experiments. In order to investigate the excited state dynamics of the C9A molecule with the nonradiative electronic couplings in a directly time-dependent manner, we propose the following intuitive scheme for a pumb-probe experiment. Consider the case where the C9A molecules are prepared initially in the symmetrical a_1 vibrational ground state of the S_0 potential. (Similarly, one could consider the a_2 state, or superpositions thereof.) First the C9A molecules are excited by a pump pulse into the S_1 state. In order to characterize the influence of the coupling to the dark S_x state in detail, we suggest that one should study series of pump pulses with different excitation frequencies such that the energy associated with this state after the laser pulse

$$E^{(1)} = \langle \psi^{(1)} | H^{(1)}_{mol} | \psi^{(1)} \rangle \tag{6}$$

can be varied. Two specific cases are a) well below and b) approximately equal to the intersection of the S_1 and S_x (Fit a) states at 26300cm^{-1}.

Two representative laser pulses are constructed as follows. In the present investigation we use a pulse of sin^2-like shape [26].

$$\varepsilon(t) = \varepsilon_0 \sin^2\left(\frac{\pi t}{\tau_p}\right) \cos(\omega t), \quad 0 \le t \le \tau_p \tag{7}$$

where ε_0 gives the amplitude of the envelope function of the electric field and ω and τ_p are the (constant) carrier frequency and the duration of the pulse, respectively. We assume a constant dipole moment function $\mu^{(1x)}$ (Condon-approximation). The duration of this laser pulse τ_p has to meet the following two conditions [27]. On the one hand, it has to be short compared to the typical time scales of vibration and S_1/S_x conversion in order to have the proper temporal resolution and not to interfere with these processes. On the other hand, it has to be long enough to obtain at least some selectivity in the population of vibrational levels of the upper electronic state because laser pulses in the impulsive limit ($\tau_p \to 0$) would excite all Condon-accessible states. As a compromise, we choose a duration of $\tau_p = 100$ fs which corresponds to a width of $1/(2\pi c \tau_p) \approx 50$ cm^{-1} in wavenumbers. Thus we expect to obtain a coherent superposition of only a few vibrational states. In order to prepare wave packets in the S_1 state such that the energy falls into the regimes a) and b) mentioned above, we desire more or less vertical transitions i.e. with the photon energy $\hbar\omega$ of the pulse roughly equal to the final energy $E^{(1)}$. Hence, the field ε_0 should not be excessively high. On the other hand, the population

$$P^{(1)} = \langle \psi^{(1)} | \psi^{(1)} \rangle \tag{8}$$

obtained in the excited S_1 state should not fall short of 10^{-2}. Figure 6 illustrates the resulting excitation by the pump process. It shows the moduli of the wave functions generated in the S_1 state at the end of the 100 fs laser pulse. The higher wavenumber $\omega/(2\pi c) = 26215$ cm^{-1} of pulse b) lies in the center of the Franck-Condon regime and thus gives rise to a nearly vertical transition of the ground state wave function. It reaches up to a wavenumber of $E^{(1)}/(hc) = 26328$ cm^{-1} which is very close to the surface crossing and it creates a population of $P^{(1)} = 13\%$ in the S_1 state. In contrast, the smaller wavenumber $\omega/(2\pi c) = 25800$ cm^{-1} of pulse a) is at the lower edge of the Condon-allowed region. This pulse

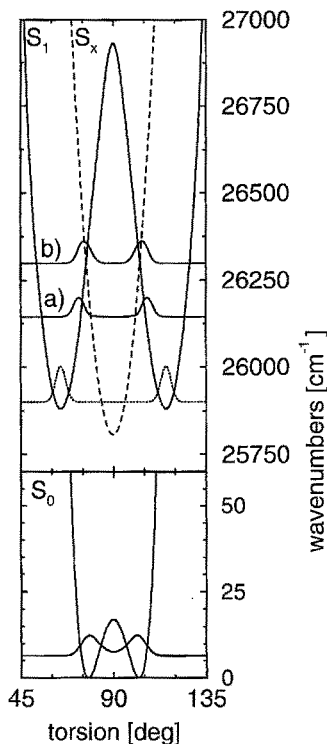**Fig. 6.** Pump laser pulse excitation $(S_0 \rightarrow S_1)$. Starting from the vibrational ground state wave function of the S_0 state, the figure shows the moduli of the wave packets generated in the S_1 state immediately after the laser pulse ($t = 100$ fs) (not drawn to scale). The parameters of the two different laser pulses a and b are given in Table 2. Also shown is the vibrational ground state wave function $\chi_0^{(1)}$ of the S_1 state

Table 2. Laser pulses for the $S_0 \rightarrow S_1$ excitation. The table gives the two sets of parameters of the pulses a) and b) as defined in (7) together with the energies $E^{(1)}$, $E^{(x)}$ and the populations $P^{(1)}$, $P^{(x)}$ of the S_1 and S_x state after the pulse, respectively

	a	b
$\omega/(2\pi c)$ [cm^{-1}]	25800	26215
ε_0 [GV/m]	0.2571	0.2571
τ_p [fs]	100	100
$E^{(1)}/(hc)$ [cm^{-1}]	26155	26328
$E^{(x)}/(hc)$ [cm^{-1}]	26271	26308
$P^{(1)}$ [%]	1.0	13.1
$P^{(x)}$ [%]	0.04	0.65

only excites some portion of the outer region of the S_0 ground state wave function and brings it up to an energy of only $E^{(1)}/(hc) = 26155$ cm^{-1} which is ≈ 150 cm^{-1} below the crossing. With a population of $P^{(1)} = 1\%$ it is still significant but clearly much less effective than pulse a). It is noted that already on the short time scale of the laser pulse ($\tau_p = 100$ fs) some population builds up in the S_x state. However, these initial populations in S_x are by a factor of 20 smaller than the corresponding values for the S_1 state. Table 2 gives an overview of the laser pulse parameters and the energies and populations of the wave functions created in the excited states.

Using the intuitive terminology of [28], the pump-probe technique can be regarded as a "snapshot" spectroscopy.

Subsequent to the pump pulse, it requires the dynamics of the "doorway" state to be probed by a second laser pulse which creates a "window" state. By choosing the time delay t and the frequency ω of the probe pulse the time and the place of this process can be controlled, respectively [28]. In a typical experiment the wave packet dynamics is monitored by ionizing the molecule [29, 30]. Since ionic potential curves for the C9A molecule are not known the probe signal is simulated in a simplified way. We assume here that the probe laser pulse is optimized such that there is a Franck-Condon window for ionization from the domain of the potential minima of the S_1 state, represented by the vibrational ground state eigenfunction $\chi_0^{(1)}$. This eigenfunction is also shown in Fig. 6 as a dotted curve. In order to monitor the passing of the excited state wave packets through the windows for ionization, we define a correlation function $C^{(1)}(t)$ as the overlap of the square of the (time-dependent) wave packet in the S_1 state $\psi^{(1)}(t)$ with the square of the (stationary) eigenfunction

$$C^{(1)}(t) = \int_0^\pi |\chi_0^{(1)}(\phi)|^2 \, |\psi^{(1)}(\phi, t)|^2 \, d\phi. \tag{9}$$

Under the assumptions given above the overlap of density associated with the propagated "doorway" state $\psi^{(1)}(t)$ with the density of the "window" state $\chi_0^{(1)}$ resembles the signal of the proposed pump-probe experiment [28].

Figure 7 shows our simulated pump-probe spectra of the C9A molecule. The upper panel illustrates the correlation
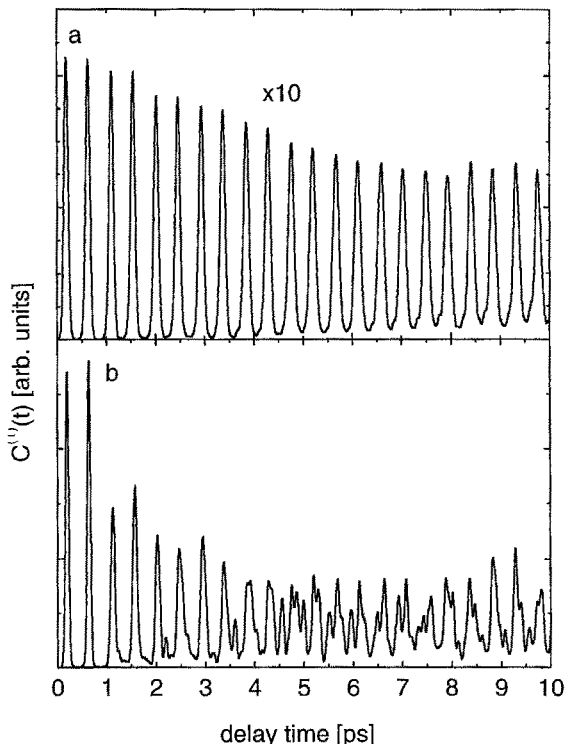

Fig. 7a, b. Model pump-probe spectra of C9A. The correlation function $C^{(1)}(t)$ defined in (9) characterizes the motion of the wave packet in the bright S_1 state. The time t denotes the time delay between the pump and probe pulses, $t = 0$ corresponds to the end of the pump laser pulse. The *upper* and *lower parts* of the figure denoted as **a** and **b** correspond to the different pump pulses shown in Fig. 6 and given in Table 2

function $C^{(1)}(t)$ for the low-wavenumber laser excitation with $\omega_0/(2\pi c) = 25800$ cm^{-1} denoted as a). Although the pump pulse was chosen to generate a wave packet below the surface crossing (see Fig. 6) there are some consequences of the diabatic transitions. The function $C^{(1)}(t)$ exhibits a slow decay of regularly spaced narrow peaks. A closer inspection of the intensity pattern reveals that there are pairs of successive maxima which have similar intensities. Starting at the inner turning point, the wave packet $\psi^{(1)}(t)$ of the bright state moves quasi-periodically towards the outer turning point and then back to the inner turning point. On its way, it passes the region of the overlap with $\chi_0^{(1)}$ after roughly one quarter and three quarters of one vibrational period which is 1 ps. It is noted that similar intensity patterns with pairs of equal peaks were also found in the pump-probe spectra of Na_2 [31]. Upon approaching the inner turning point there is some leakage of probability from the S_1 to the S_x state in the range of the diabatic potential coupling. This explains the slight drop of intensity after every second peak. However, even for the case of vanishing potential coupling there is a continuous spreading of the wave packet due to the anharmonicity of the potential. Test calculations showed that the first partial revival of the initial shape of the wave packet occurs only after more than 100 ps. Therefore, fractional revivals [32] do not play a role on the time scale of 10 ps considered here.

The effects of the diabatic curve crossing are much more drastic for case b) of the high-wavenumber pump laser pulse with $\omega_0/(2\pi c) = 26215$ cm^{-1}. The second pair of maxima of the function $C^{(1)}(t)$ only reaches half the intensity of the first one. After a few more vibrational periods there is a rapid loss of structure in the simulated ion signal which is due to interference of wave packet motions in the S_1 and S_x states which interact much more strongly for this case. This transition of the structure of the pump-probe spectra as a function of the pump pulse wavelength may also serve to determine the potential coupling.

6 Conclusions

The present paper studies the excited state dynamics of the C9A molecule using a diabatic representation of the electronic states. The effects of non-radiative transitions from the bright S_1 state to a dark "S_x" state are investigated by means of time-independent and time-dependent spectroscopy. As a first step, we set up an approximate one-dimensional model Hamiltonian for the torsional degree of freedom, only. Based on calculated Franck-Condon factors, we fit a quartic potential for the dark state and a simple diabatic coupling function to the experimental fluorescence excitation spectrum. The position of the surface crossing as well as the strength and the width of the coupling function can be determined accurately. However, the differences in the resulting two sets of the remaining fit parameters indicate some uncertainties of such a fit procedure. Nevertheless, these empirical potentials may serve as a challenging reference for future accurate ab-initio work on excited state potentials for the C9A molecule. Moreover, these calculations still have to address the question of the charge transfer (TICT) nature of the "S_x" state which was suggested in [9].

Other effects of non-radiative coupling of the bright to the dark state predicted in our calculations are the partial lifting of the degeneracy of the a_1 and a_2 levels and the intensity borrowing of the S_x state. The absence of both effects points to additional nonradiative decay mechanisms starting from the S_x state which are beyond our description using a one-dimensional model Hamiltonian with three electronic states. However, it is planned to extend our model to include more degrees of freedom to model the effects of vibrational mode coupling of electronic states and intramolecular vibrational energy redistribution (IVR). Recently, Seidner et al. studied the effects of mode couplings on internal conversion processes using models for torsional photoisomerizations with up to four nuclear degrees of freedom [15, 16]. Finally we plan to model the C9A torsion using a density matrix description. In this approach the effect of competing processes such as IVR in S_1 and S_x as well as solvation effects on the torsional spectra and dynamics can also be studied, see e.g. [33].

Based on this model Hamiltonian and the electronic potential curves, we suggest a pump-probe scheme to investigate the excited state torsional dynamics of C9A in a directly time-dependent manner. A monochromatic 100 fs laser pulse is used to generate a wave packet in the electronically excited S_1 state. Then the time evolution of this non-stationary "doorway" state is probed assuming that ionization takes place only from the "window" region where the vibrational ground state wave function of S_1 is localized. Our model calculations clearly demonstrate the influence of the surface crossing on the time dependence of the probe signal. For pump laser excitations below the intersections of the S_1 and the S_x potential, there is a regular periodic probe signal while for pumping with higher frequency the structure of the probe signal is lost due to non-radiative transitions to the S_x state. This work may serve as a guideline for future pump-probe experiments. By tuning the frequency of the pump laser, the position of the potential surface crossing should be directly detectable in the structure of the probe (ion) signal.

References

1. Michl, J., Bonačić-Koutecký, V.: Electronic aspects of organic photochemistry. New York: Wiley 1990
2. Lippert, E., Lüder, W., Boos, H.: In: Advances in molecular spectroscopy. p. 443. Mangini A. (ed.). Oxford: Pergamon Press 1962
3. Grabowski, Z.R., Rotkiewicz, K., Siemiarczuk, A., Cowley, D.J., Baumann, W.: Nouv. J. Chim. 3, 443 (1979)
4. Lippert, E., Rettig, W., Bonačić-Koutecký, V., Heisel, F., Miehé, J.A.: Adv. Chem. Phys. 68, 1 (1987)

118

5. Rettig, W.: In: Electron transfer I. Mattay, J. (ed.). Topics in current chemistry, Vol. 169, pp. 253–299. Berlin Heidelberg New York: Springer 1994
6. Subaric-Leitis, A., Monte, C., Roggan, A., Rettig, W., Zimmermann, P.: J. Chem. Phys. **93**, 4543 (1990)
7. Kajimoto, O., Yamasaki, K., Arita, K., Hara, K.: Chem. Phys. Lett. **125**, 184 (1986)
8. Honma, K., Arita, K., Yamasaki, K., Kajimoto, O.: J. Chem. Phys. **94**, 3496 (1991)
9. Monte, C., Roggan, A., Subaric-Leitis, A., Rettig, W., Zimmermann, P.: J. Chem. Phys. **98**, 2580 (1993)
10. Quack, M.: Annu. Rev. Phys. Chem. **41**, 839 (1990)
11. Quack, M.: In: Femtosecond chemistry, Chap. 27. Manz, J., Wöste, L. (eds.). Weinheim: Verlag Chemie 1995
12. Frederick, J.H., Heller, E.J., Ozment, J.L., Pratt, D.W.: J. Chem. Phys. **88**, 2169 (1988)
13. Lewis, J.D., Malloy, T.B., Taina, H., Lacane, C., Lacane, J.: J. Mol. Struct. **12**, 427 (1972)
14. Dormans, G.J.M., Groenenboom, G.C., Buck, H.M.: J. Chem. Phys. **86**, 4895 (1987)
15. Seidner, L., Stock, G., Domcke, W.: Chem. Phys. Lett. **228**, 665 (1994)
16. Seidner, L., Domcke, W.: Chem. Phys. **186**, 27 (1994)
17. Kosloff, R.: J. Phys. Chem. **92**, 2087 (1988)
18. Meyer, R.: J. Chem. Phys. **52**, 2053 (1970)
19. Marston, C.C., Balint-Kurti, G.G.: J. Chem. Phys. **91**, 3571 (1989)
20. Leforestier, C., Bisseling, R.H., Cerjan, C., Feit, M.D., Friesner, R., Guldberg, A., Hammerich, A., Jolicard, G., Karrlein, W., Meyer, H.-D., Lipkin, N., Roncero, O., Kosloff, R.: J. Comp. Phys. **94**, 59 (1991)
21. Kosloff, R.: Annu. Rev. Phys. Chem. **45**, 145 (1994)
22. Feit, M.D., Fleck, Jr, J.A., Steiger, A.: J. Comput. Phys. **47**, 412 (1982)
23. Feit, M.D., Fleck, Jr, J.A.: J. Chem. Phys. **78**, 301 (1983)
24. Alvarellos, J., Metiu, H.: J. Chem. Phys. **88**, 4957 (1988)
25. Tal-Ezer, H., Kosloff, R.: J. Chem. Phys. **81**, 3967 (1984)
26. Paramonov, G.K., Savva, V.A.: Phys. Lett. **A97**, 340 (1983)
27. Stock, G., Domcke, W.: Phys. Rev. **A45**, 3032 (1992)
28. Mukamel, S.: Annu. Rev. Phys. Chem. **41**, 647 (1990)
29. Khundkar, L.R., Zewail, A.H.: Annu. Rev. Phys. Chem. **41**, 15 (1990)
30. Zewail, A.H.: In: Femtosecond chemistry, Chap. 2. Manz, J., Wöste, L. (eds.). Weinheim: Verlag Chemie 1995
31. Meier, C., Engel, V.: In: Femtosecond chemistry, Chap. 11. Manz, J., Wöste, L. (eds.). Weinheim: Verlag Chemie 1995
32. Averbukh, I.S., Perelman, N.F.: Phys. Lett. **A139**, 449 (1989)
33. Kühn, O., May, V.: Chem. Phys. Lett. **225**, 511 (1994)